Research Square

Preprints are preliminary reports that have not undergone peer review.
They should not be considered conclusive, used to inform clinical practice,
or referenced by the media as validated information.

Association of Unsaturated Fatty Acid–Related Immunometabolic Features with Differential Responses to Erenumab in Patients with Migraine: An Exploratory Multi-Omics Study

Rong Wu
Shanghai Jiao Tong University
Jiaqi Fu
Shanghai Jiao Tong University
Qianfeng Yan
Shanghai Jiao Tong University
Yuanyuan Zeng
Shanghai Jiao Tong University
Tingting Wu
Shanghai Jiao Tong University
Xueyuan Liu
Shanghai Jiao Tong University
Li Gong
gongli0808@sjtu.edu.cn
Shanghai Jiao Tong University

Research Article

Keywords: migraine, erenumab, treatment response, whole-blood transcriptomics, untargeted metabolomics, unsaturated fatty acids, weighted gene co-expression network analysis

Posted Date: November 1st, 2026

DOI: https://doi.org/10.21203/rs.3.rs-11353910/v1

License: This work is licensed under a Creative Commons Attribution 4.0 International License. Read Full License

Additional Declarations: No competing interests reported.

Abstract

Background

Erenumab, the first calcitonin gene-related peptide (CGRP) receptor-targeting monoclonal antibody approved for migraine prevention in China, has shown substantial clinical benefit in Chinese patients with migraine. However, the degree of improvement varies among individuals. We therefore investigated pretreatment metabolic and transcriptional features associated with differences in erenumab response.

Methods

In this prospective study, 40 patients with migraine received erenumab 70 mg every 4 weeks for 3 months. Pretreatment whole-blood samples underwent untargeted metabolomics and RNA sequencing. Super-response was defined as a ≥ 75% reduction in monthly headache days at month three; patients not meeting this criterion were classified as non-super-responders. Analyses integrated differential feature screening, metabolite-set enrichment, a UFA-related principal component score, weighted gene co-expression network analysis, and response-group-adjusted gene–metabolite correlations. Molecular docking was exploratory.

Results

26 patients (65%) achieved super-response. We identified 52 differential metabolomic features and 297 candidate differentially expressed genes. UFA biosynthesis was enriched toward non-super-responders (normalized enrichment score 2.12; P = 0.00118). Four transcriptional modules were associated with the metabolic score, and 14 genes overlapped these modules and the differential expression set. Across 84 gene–metabolite correlations, the feature annotated as strophanthidin was inversely associated with PREX1, MYADM, BCL3, and KDM6B (partial rho − 0.52 to − 0.48; P = 0.0418 for each). These four genes showed higher expression in non-super-responders than in super-responders. Gene-centered enrichment identified overlapping pathways related to immune function, and exploratory docking characterized potential interactions between erenumab and proteins encoded by the four candidate genes.

Conclusions

We identified UFA-related metabolic variation associated with non-super-responder versus super-responder status in erenumab-treated migraine patients. Four candidate genes were inversely associated with a shared mass-spectrometry feature. These findings provide new molecular insights into response heterogeneity and potential directions for further investigation.

Background

Migraine is a disabling neurological disorder for which calcitonin gene-related peptide (CGRP)-targeted treatment has expanded preventive options [1]. Erenumab, a monoclonal antibody against the CGRP receptor, was the first CGRP receptor-targeting monoclonal antibody approved in China for migraine prevention [2]. Its efficacy has been demonstrated in international and Asian clinical trials, including studies enrolling patients from China [3–8]. In our clinical practice, erenumab has also shown substantial clinical benefit, although the magnitude of improvement varies considerably among patients.

Previous studies have reported considerable variability in the proportion of patients achieving pronounced improvement with erenumab, although direct comparisons are limited by differences in response definitions, follow-up duration, and patient characteristics [9–11]. These observations raise an important question: why do some patients achieve exceptionally marked benefits while others respond less favorably to the same treatment? Although erenumab has shown encouraging efficacy in Chinese patients and has entered clinical practice in China, studies examining the biological features associated with this response heterogeneity in Chinese patients remain limited. This clinical observation and evidence gap motivated us to investigate pretreatment molecular patterns linked to different degrees of improvement.

Circulating small-molecule metabolites may provide clues to this variation. Migraine has been linked to energy metabolism, lipid signaling, and other systemic metabolic processes [12]. Dietary modification of n-3 and n-6 fatty acids has also improved headache outcomes in a randomized trial [13]. We therefore first performed untargeted metabolomics on pretreatment blood samples from SR and NSR patients to identify differential features and enriched metabolic pathways. Because metabolite abundance alone cannot establish its underlying molecular regulation, we next analyzed pretreatment whole-blood transcriptomes to identify differential genes and associated functional programs.

We then integrated the two datasets to determine whether response-associated metabolites and transcripts converged on shared molecular candidates. Differential expression, weighted gene co-expression network analysis, and gene–metabolite correlations provided a stepwise route from metabolic pathways to prioritized genes [14]. Finally, we explored structural models and potential interfaces between erenumab and four candidate proteins using molecular docking. These predictions were intended to generate testable hypotheses, not to establish physical binding or competitive inhibition.

This prospective exploratory study aimed to characterize baseline metabolic and transcriptional features associated with erenumab super-response, identify molecular candidates supported by both omics layers, and assess their possible structural relevance to interindividual treatment response.

Methods

Study design and analytical question

This prospective, single-center observational cohort was conducted at Tongren Hospital, Shanghai Jiao Tong University School of Medicine, Shanghai, China. Consecutive enrollment occurred from September 2025 to March 2026 (ClinicalTrials.gov identifier: NCT05334927; registration first posted on 19 April 2022). Baseline blood collection preceded the first erenumab injection, and response was assessed after three months. Analysis required paired baseline transcriptomic and metabolomic profiles and an available month-three outcome. Reporting follows the Strengthening the Reporting of Observational Studies in Epidemiology statement [15].

The study compared outcome-defined response strata among adults receiving erenumab 70 mg every four weeks in routine care. The outcome was percentage reduction in monthly headache days from the baseline month to month three; no untreated, placebo, or healthy comparator was included. The observational design evaluated pretreatment molecular measurements against a subsequent clinical outcome within the same treatment regimen. Response strata were defined by improvement, rather than by a molecular classification.

Participants and treatment response

Adults diagnosed using the International Classification of Headache Disorders, third edition, were eligible with or without aura [16]. Eligibility required frequent episodic migraine with ≥ 8 headache days monthly or chronic migraine with ≥ 15 headache days monthly. Clinicians selected erenumab before molecular profiling; treatment decisions did not use molecular measurements. The analysis population additionally required both molecular assays and an ascertainable month-three response, ensuring that each included participant contributed matched clinical and molecular information.

All 40 analyzed participants completed three subcutaneous injections of erenumab 70 mg at four-week intervals; other medications were maintained without planned changes. Patients reported monthly headache days (MHD) at baseline and the three-month visit. Baseline MHD covered the pretreatment month, and follow-up MHD was the month-three count, rather than an average across treatment months. Improvement was calculated as 100 × (baseline MHD − month-three MHD)/baseline MHD. Super-responders (SR) achieved ≥ 75% improvement; non-super-responders (NSR) achieved < 75%, including partial benefit.

Baseline variables were age, sex, MHD, Migraine Disability Assessment (MIDAS), and six-item Headache Impact Test (HIT-6) scores [17, 18]. Molecular contrasts consistently compared NSR with SR: positive log2 fold changes indicate higher abundance or expression in NSR, and negative values indicate higher levels in SR. Clinical scores were descriptive measures of disability and headache impact and were not used in molecular candidate selection. The contrast orientation was identical in both omics layers.

Baseline sampling and laboratory workflow

Fasting interictal whole blood was collected before the first injection into dipotassium ethylenediaminetetraacetic acid (K2EDTA) tubes and stored at − 80°C. Specimens remained frozen until cohort collection was complete and were shipped together for analysis. Transcriptomics and metabolomics used the same baseline whole-blood source; no follow-up molecular measurements were included.

Novogene Co., Ltd. (Beijing, China) performed RNA sequencing and untargeted metabolomics. Downstream inputs comprised gene-count and expression matrices, metabolite annotations, and relative abundance matrices. A participant-mapping table linked both assays to clinical response. Only paired baseline measurements were analyzed. Measurements from different visits were not combined, and post-treatment specimens were not substituted for missing baseline samples. The mapping table was used throughout the paired analyses.

Untargeted metabolomics and feature annotation

Whole-blood aliquots underwent cold methanol extraction, protein precipitation, incubation on ice, and refrigerated centrifugation. Supernatants were diluted with mass-spectrometry-grade water and clarified by a second centrifugation before liquid chromatography–mass spectrometry.

Ultra-high-performance liquid chromatography–Orbitrap Exploris 120 mass spectrometry acquired positive- and negative-ion data, with pooled quality-control (QC) specimens monitoring analytical stability. ProteoWizard converted raw files; XCMS performed peak detection, retention-time alignment, and peak-area extraction [19, 20]. Normalization followed the laboratory total-peak-area and QC-based workflow.

Peaks with > 50% missing observations, blank-derived background, or QC coefficient of variation > 30% were excluded; remaining missing values underwent k-nearest-neighbor imputation. Compound assignment combined accurate mass and adduct information (10 parts per million tolerance) with NovoMetDB tandem mass-spectral matching. KEGG, HMDB, and LIPID MAPS supplied annotations. Vendor annotation levels 1 and 2 were retained; authentic-standard and retention-time confirmation was not independently established for every feature [21, 22].

Ion modes were analyzed separately after log2(x + 1) transformation and exclusion of nonfinite or zero-variance features. The retained matrices contained 1,050 positive-ion and 630 negative-ion features. Differential screening used ion-mode-specific signals; compound-level analyses aggregated signals as described below. Because one compound may produce several signals or occur in both modes, feature counts describe screened analytical signals rather than independently confirmed chemical substances.

Differential metabolite screening

Within each ion mode, limma compared NSR with SR using a response-group-only design and empirical-Bayes variance moderation [23]. Orthogonal partial least-squares discriminant analysis used ropls, one predictive and one orthogonal component, and seed 2410 [24]. Differential metabolite features (DEMs) required variable importance in projection (VIP) > 1 and nominal limma $P < 0.05$. Benjamini–Hochberg-adjusted probabilities were retained but did not determine screening [25].

VIP and limma used the same response labels, making feature selection exploratory. Volcano plots used log2 fold change and −log10 nominal P. Heatmaps displayed up to 20 features per direction in each ion mode, with standardized transformed abundances clipped at ± 2. The display limit meant that some screened features were absent from the positive-ion heatmap. Selected-feature separation was used for visualization and was not evaluated as predictive accuracy.

Metabolite set enrichment and the unsaturated fatty acid score

Metabolite set enrichment used KEGG compound–pathway relationships [26]. Features with valid KEGG identifiers were transformed and standardized, then averaged by compound across signals and ion modes. Pathway sets were restricted to measured compounds. Broad overview maps were excluded; eligible sets contained 3–100 measured compounds. Aggregation occurred at the standardized-abundance level, giving one compound-by-participant matrix for both ranked analyses. Unmeasured pathway components did not contribute to enrichment calculations.

Enrichment used clusterProfiler with the fgsea backend [27, 28]. Phenotype-ranked analysis ordered compounds by the limma NSR-versus-SR statistic. DEM-centered analysis ranked compounds by partial Spearman correlation with each KEGG-mapped differential seed, adjusting for response group and excluding the seed itself. Tables retained normalized enrichment scores (NES), P values, and leading-edge compounds. Display criteria were nominal $P < 0.05$ and $|NES| > 1$. Adjustment applied within each run, rather than across all seeds or selection stages.

Unsaturated fatty acid (UFA) biosynthesis (KEGG hsa01040) was enriched in both the phenotype-ranked and DEM-centered analyses. Eight compounds were present in the phenotype-ranked leading edge and in at least one DEM-centered leading edge. PCA of their standardized abundances defined the UFA score as PC1, with the sign oriented so that the sum of loadings was positive.

The UFA score summarizes coordinated abundance among these compounds, not biosynthetic flux. Because the constituent compounds were selected in the discovery cohort, its group-wise distribution is descriptive.

RNA library preparation and data processing

mRNA was enriched using oligo(dT)-conjugated beads, fragmented, and reverse-transcribed with random hexamers to generate double-stranded cDNA. Libraries were prepared by end repair, adenylation, adapter ligation, size selection, amplification, and purification. Before pooling, libraries that passed supplier quality control were assessed by fluorometry, quantitative PCR, and fragment-size analysis.

Illumina FASTQ reads were processed with fastp [29]. Adapter-contaminated reads were removed. For paired reads, a pair was discarded if either read contained > 10% undetermined bases or > 50% bases with Phred quality ≤ 5. Sequencing quality was summarized using Q20, Q30, and GC content. Based on GENCODE version 36 annotations, protein-coding genes were retained with one entry per gene symbol. Gene-count and FPKM matrices were used as downstream inputs. Raw counts were used for differential expression, whereas preprocessed expression values were used for visualization, networks, and rank correlations.

Matrices were aligned to the same 40 participants. Sample correspondence was rechecked at the pathway-score, network-trait, and gene–metabolite stages. Patient identifiers were excluded from figures and reported tables. These steps ensured participant-level correspondence when the two assays were combined, including after feature filtering and before calculation of the metabolic score and cross-omics correlations.

Differential expression and co-expression networks

Rounded protein-coding counts were analyzed with DESeq2 using a response-group-only design and the NSR-versus-SR contrast [30]. Age and sex were comparable between response groups; therefore, models were not adjusted for age, sex, batch, or cell fractions. Genes with non-estimable P values were excluded before screening. Genes were screened at nominal $P < 0.05$ and $|\log2 \text{ fold change}| > 0.5$, and adjusted P values were retained for reference. The candidate differential-expression set was defined by the nominal rule; adjusted P values were not used to define this set. Heatmaps showed up to 20 genes per direction using row-standardized expression clipped at ± 2.

WGCNA was performed on protein-coding genes with expression > 1 in at least half of samples after $\log2(x + 1)$ transformation. We selected the 5,000 genes with the greatest median absolute deviation, regressed out PC1 from centered and scaled expression, and used the residuals as network input. A signed network was built with biweight midcorrelation and signed topological overlap, and soft-threshold power 12 was selected to achieve a signed scale-free fit of 0.80. Modules were detected using standard WGCNA settings. Module eigengenes were correlated with participant-matched UFA PC1; modules with $|r| \geq 0.30$ and $P < 0.05$ were retained. Their genes were intersected with the differential-expression set, yielding 14 candidates, with no additional module-membership or gene-significance thresholds.

Gene–metabolite correlations and functional annotation

Cross-omics analysis retained DEMs either directly mapped to hsa01040 or meeting the exploratory hsa01040 enrichment criterion in seed-centered rankings, with these categories recorded separately. Six metabolite features, including one direct pathway member, were paired with 14 candidate genes, yielding 84 tests across 40 participants. Measurements were rank-transformed using average ranks for ties, and the effects of binary response group were removed by linear regression. Pearson correlations between the resulting residuals defined group-adjusted partial Spearman rho. Two-sided P values were calculated using a t approximation with n − 3 degrees of freedom, followed by Benjamini–Hochberg correction across all 84 tests. Candidate pairs were prioritized using |partial rho| > 0.40 and P < 0.05. Unadjusted Spearman correlations were retained for reference; covariate adjustment was limited to response group.

The 14 candidate genes underwent Gene Ontology (all three ontologies) and KEGG over-representation analysis using clusterProfiler, human annotation resources, and offline graphite KEGG gene sets [28]. An annotation-defined background was used. Enriched terms were presented with contributing genes to assess the extent of shared or single-gene support.

For each of the four prioritized genes, all measured genes were ranked by their Spearman expression correlations across the cohort without response-group adjustment. Rank-based enrichment was performed using clusterProfiler and human MSigDB KEGG legacy gene sets (version 2026.1) [27, 31]. The five pathways with the largest absolute normalized enrichment scores (|NES|) among those meeting P < 0.05 were displayed for each candidate. These analyses characterized candidate-associated co-expression programs rather than differential expression between response groups and did not establish regulatory direction.

Exploratory structural modeling

Four candidate proteins (BCL3, KDM6B, MYADM, and PREX1) were subjected to exploratory molecular docking with the antigen-binding variable fragment (Fv) of erenumab using HADDOCK3 [32, 33]. The erenumab heavy- and light-chain variable regions were obtained from the crystal structure PDB 6UMG [34]. Available structural domains were used for BCL3, KDM6B, and PREX1, whereas a full-length AlphaFold-predicted structure was used for MYADM [35, 36].

For each candidate protein, 1,000 initial rigid-body docking poses were generated using a fixed random seed of 917. Of these, 200 poses underwent flexible refinement followed by energy minimization. Docking incorporated ambiguous interaction and intramolecular restraints. The resulting configurations were clustered using the fraction-of-common-contacts method (cutoff, 0.6; minimum cluster size, 4; contact distance threshold, 5 Å), and representative configurations were selected for structural analysis.

Representative models were examined to characterize predicted protein–antibody interfaces, including residue-level contacts, hydrogen bonds, and electrostatic interactions. These analyses were used to generate exploratory hypotheses regarding potential interaction interfaces.

Statistical interpretation and reproducibility

Continuous baseline variables were summarized as means and standard deviations, and categorical variables as counts and percentages. Baseline comparisons were descriptive. Statistical significance was evaluated using the prespecified criteria for each analysis.

Analyses used R 4.3.3, DESeq2 1.40.2, WGCNA 1.73, limma 3.56.2, ropls 1.32.0, clusterProfiler 4.15.0.3, fgsea 1.26.0, and graphite 1.46.0. Metabolomic and gene-enrichment scripts used seed 2410. No held-out prediction model was developed, so discrimination, calibration, decision thresholds, and clinical utility were not estimated [37].

Sample size was determined by the available participants with paired molecular profiles and month-three outcomes, without a prospective molecular power calculation. Entirely missing assays were not imputed; missing metabolite signals were imputed using the supplier-provided method. Analysis scripts and figure-level result tables were retained to support reproducibility.

Results

Cohort and response distribution

The study workflow comprised baseline whole-blood collection, treatment with erenumab, assessment of the month-three clinical outcome, and integration of the paired molecular profiles (Fig. 1a). A total of 43 patients were enrolled in the cohort. Two patients provided baseline blood samples but were lost to follow-up; their samples were therefore not sequenced. One additional patient was excluded because of sample degradation, leaving 40 patients for the paired molecular analysis. All molecular profiles were generated from blood samples collected before erenumab treatment. Twenty-six patients (65%) achieved at least a 75% reduction in MHD and were classified as SR. The remaining 14 patients (35%) were classified as NSR. The individual-response waterfall illustrates the range of improvement relative to the 75% threshold (Fig. 1b).

Baseline demographic and clinical characteristics of the SR and NSR groups, including age, sex distribution, MHD, MIDAS scores, and HIT-6 scores, are summarized in Fig. 1c. The NSR group included patients with partial clinical benefit as well as those with little improvement, all of whom had an MHD reduction below 75%.

Metabolomic Profiling Identifies Differential Features and UFA-Related Enrichment

To examine pretreatment metabolic differences associated with subsequent erenumab response, we compared baseline untargeted metabolomic profiles between SR and NSR. The analysis retained 630 negative-ion and 1,050 positive-ion features. Screening with VIP > 1 and nominal P < 0.05 identified 52 ion-mode-specific differential features: 16 in negative-ion mode and 36 in positive-ion mode. Nine negative-ion and 14 positive-ion features were higher in NSR, whereas seven and 22, respectively, were higher in SR (Fig. 2a–d).

At the compound level, enrichment analysis of the NSR–SR ranking highlighted unsaturated fatty acid (UFA) biosynthesis, which showed the strongest positive enrichment among the displayed pathways. The pathway contained 12 measured compounds and was enriched toward NSR (NES = 2.12; P = 0.00118; Fig. 2e).

UFA biosynthesis also showed recurrent nominal enrichment across several differential-feature-centered analyses after adjustment for SR/NSR group membership (Fig. 2f). Positive enrichment was observed for features annotated as stearamide, cis-13,16-docosadienoic acid, and panthenol, whereas the feature annotated as strophanthidin showed negative enrichment. These findings linked several differential features to coordinated variation in UFA-pathway compounds and motivated further characterization of this metabolic pattern.

Eight measured UFA-pathway compounds formed a common core, each contributing to the phenotype-ranked leading edge and at least one nominally enriched differential-feature-centered leading edge. This common core included annotations corresponding to homo-γ-linolenic acid, α-linolenic acid, arachidonic acid, linoleic acid, and other long-chain unsaturated fatty acids. The first principal component of their standardized abundances was used as the UFA signature.

UFA PC1 values were higher in NSR than in SR, although the individual distributions overlapped substantially (Fig. 2g). This comparison was exploratory because the pathway and signature components had been selected within the same cohort. We next used the UFA PC1 score as a continuous metabolic trait to examine associated transcriptional programs in the paired pretreatment gene-expression profiles

Transcriptomic Analysis Identifies Differential Genes and UFA-Associated Co-expression Modules

To investigate transcriptional programs that might accompany the UFA-associated metabolic pattern, we next combined response-group differential-expression analysis with co-expression network analysis anchored to the UFA score. DESeq2 returned estimable nominal probabilities for 13,167 genes. The nominal P below 0.05 and absolute log2 fold change above 0.5 rule selected 297 genes, of which 206 were higher in NSR and 91 higher in SR. Figure 3a shows the full tested distribution, while Fig. 3b displays the selected genes with the largest fold changes in each direction. The heatmaps visualize the group contrast used to select these genes. The 297-gene set was the input to the differential-expression component of the subsequent intersection analysis.

Following expression-PC1 regression, WGCNA identified 29 modules from the 5,000 most variable eligible genes (Fig. 3c,d). Four modules met the exploratory correlation and nominal P-value criteria for association with the UFA PC1 score. Cyan (r = 0.42, P = 0.00673) and grey60 (r = 0.41, P = 0.00863) showed positive associations. Pink (r = − 0.39, P = 0.0121) and green (r = − 0.34, P = 0.0306) showed negative associations.

The four selected modules contained 736 genes. Intersecting these genes with the 297 genes identified by nominal differential-expression screening between SR and NSR yielded 14 candidates (Fig. 3e). These candidates were MYG1, TLR9, TP53I11, ERGIC1, FHL3, IFI44, B9D2, MYADM, BCL3, PREX1, KDM6B, KRT1, CFAP36, and EBPL. This overlap prioritized genes associated with both response-group differences and coordinated transcriptional variation linked to the UFA score.

Functional annotation of the 14 candidates highlighted cytokine regulation, adhesion-dependent cell spreading, NF-κB-related complexes, and histone demethylase activity (Fig. 3f). TLR9 and BCL3 contributed to terms involving the regulation of interleukin-8 and interleukin-10 production. MYADM and PREX1 supported cell-spreading annotations, whereas KDM6B contributed to H3K27 demethylase terms. Most displayed KEGG terms, including several infection-related annotations, were supported by TLR9 alone. Collectively, these annotations highlighted immune regulation, cell adhesion, and chromatin regulation within the prioritized candidate set.

Cross-Omics Integration Prioritizes Four Genes Associated with a Strophanthidin-Annotated Feature

To connect the UFA-related metabolic pattern with the 14 transcriptional candidates, we examined their associations with six selected differential metabolite features. These features were annotated as strophanthidin, glycolithocholic acid 3-sulfate, stearamide, 3-ethyltoluene, panthenol, and cis-13,16-docosadienoic acid. Of these, cis-13,16-docosadienoic acid mapped directly to UFA biosynthesis (hsa01040), whereas the other five features were linked through differential-feature-centered enrichment.

Of the 84 gene–metabolite pairs tested, four met the prespecified selection criteria, all involving the positive-ion feature Com_1326_pos, putatively annotated as strophanthidin (Fig. 4a). This feature was more abundant in SR than in NSR. After accounting for response group, partial Spearman correlations were − 0.517 for PREX1, − 0.497 for MYADM, − 0.485 for BCL3, and − 0.480 for KDM6B. Nominal P values for all four associations were below 0.002.

PREX1, BCL3, and KDM6B belonged to the cyan module, whereas MYADM belonged to grey60. The shared inverse associations therefore involved genes from both modules positively associated with the UFA score. The chemical identity of Com_1326_pos remains provisional, and its connection to UFA biosynthesis reflects correlation-based enrichment.

Across the cohort, GSEA of gene-centered correlation rankings identified overlapping pathways associated with the four candidates (Fig. 4b–e). Glycosaminoglycan degradation was positively enriched in all four rankings (NES 2.12–2.25), and Fc gamma receptor-mediated phagocytosis appeared among the leading displayed pathways for each gene. The citrate cycle was prominent in the PREX1 (NES = 2.37), MYADM (NES = 2.23), and KDM6B (NES = 2.07) rankings. BCL3-associated rankings additionally highlighted lysosome and Notch signaling, while the MYADM and PREX1 rankings included proteasome and neurotrophin signaling, respectively. These shared enrichments placed the four candidates within a common transcriptional context involving immune and cellular metabolic processes.

Exploratory Docking of Four Candidate Proteins with Erenumab

To explore potential structural contacts between erenumab and the proteins encoded by the four cross-omics candidate genes, we performed exploratory molecular docking using HADDOCK3. BCL3, KDM6B, MYADM, and PREX1 were individually docked against the paired heavy- and light-chain variable regions of erenumab. The representative refined models displayed distinct interfaces containing putative hydrogen bonds and electrostatic contacts (Fig. 5a–d). In the BCL3 model, Glu125 contacted erenumab Lys113, while Arg155 formed putative hydrogen bonds with Tyr104 and Asp105 (Fig. 5a). The KDM6B interface included putative hydrogen bonds linking Asn1391 to erenumab Asp105 and Ala1493 to Gly199 (Fig. 5b).

In the MYADM model, Tyr261, Gln270, and Arg281 formed putative hydrogen bonds with erenumab Tyr110, Ser107, and Asn161, respectively (Fig. 5c). Additional predicted electrostatic contacts involved MYADM His199–erenumab Asp54 and MYADM Asp276–erenumab His111. For PREX1, predicted contacts included Glu245–erenumab Lys113 and Arg403–erenumab Asp54, alongside a putative hydrogen bond between Cys269 and erenumab Ser107 (Fig. 5d). Across the four representative models, erenumab Asp54 and residues within the 104–113 region repeatedly contributed to the predicted interfaces.

Discussion

This prospective study applied a metabolomics-led multi-omics approach to explore variation in response to erenumab among Chinese patients with migraine. Untargeted metabolomic profiling first highlighted an unsaturated fatty acid (UFA)-related pattern, which was summarized using a pathway-derived score. Subsequent transcriptomic analysis identified response-associated expression changes and co-expression modules linked to this metabolic trait. Integrating these results yielded 14 candidate genes, and correlations with six previously selected metabolite features further prioritized PREX1, MYADM, BCL3, and KDM6B. These genes shared inverse associations with a metabolomic feature annotated as strophanthidin. Gene-centered enrichment and exploratory docking of the corresponding proteins then extended the patient-level findings to functional and structural hypotheses. This strategy identifies specific molecular relationships within a broader metabolic and transcriptional pattern associated with the depth of clinical improvement.

After three months, 26 of 40 patients achieved a reduction of at least 75% in monthly headache days. In a RCT(The DRAGON trial and its recent extension provide evidence of erenumab's clinical benefit in Asian populations, including Chinese patients [7, 38]. In our study, the 75% threshold enabled examination of particularly pronounced improvements within a cohort receiving the same 70-mg regimen. Recent clinical research has also developed tools based on baseline clinical characteristics for estimating treatment response [39]. Our approach adds a molecular dimension to this clinical literature by examining pretreatment features measured in the same patients before subsequent response was assessed.

The UFA-related pattern was the starting point of this integration. UFA biosynthesis was enriched toward non-super-responders (normalized enrichment score = 2.12; nominal P = 0.00118), and the score derived from eight shared leading-edge compounds was relatively higher in this group. The core included annotations corresponding to α-linolenic, linoleic, arachidonic, and other long-chain unsaturated fatty acids. These compounds participate in biologically diverse lipid processes, suggesting that their coordinated abundance may capture aspects of lipid composition relevant to migraine. A recent JHP multi-omics study reported relationships between migraine-associated plasma proteins and lipid-metabolomic measures [40]. Additionally, a randomized dietary study showed reductions in headache days after modifying n-3 and n-6 fatty acid intake [13]. These observations provide a biological context for considering lipid-related molecular states when studying differences in preventive-treatment outcomes.

Subsequent whole-blood transcriptomic profiling identified 297 candidate differentially expressed genes and 29 co-expression modules. Four modules were selected according to their associations with the UFA score, and their overlap with the response-associated gene set yielded 14 candidates. Functional annotations involving cytokine regulation, cell adhesion, and chromatin regulation suggested that lipid-associated variation may be accompanied by coordinated transcriptional changes, including selected immune-related processes. Recent JHP proteomic research and experimental studies together implicate neuroimmune processes in migraine and show that sensory neuron-derived CGRP regulates neutrophil and macrophage functions [41, 42]. Together, these findings suggest a potential relationship between lipid-associated baseline variation and broader transcriptional regulatory processes in the setting of CGRP receptor blockade.

The most specific cross-omics result emerged from correlations between the 14 genes and six metabolomic features selected earlier in the workflow. Com_1326_pos, annotated as strophanthidin, showed inverse response-group-adjusted associations with PREX1, MYADM, BCL3, and KDM6B. PREX1, BCL3, and KDM6B originated from the cyan module, while MYADM came from grey60; both modules were positively associated with the UFA score. The feature's relationship to UFA-related variation was identified through metabolite-centered enrichment. These convergent associations define four measurable gene–metabolite pairs and narrow the multi-omics observations to a set of candidates for targeted study.

The biological functions of these four genes suggest links between metabolic variation, inflammatory regulation, membrane signaling, and cellular behavior. BCL3 participates in inflammatory transcriptional regulation and has been linked experimentally to macrophage glycolysis and polarization [43]. KDM6B connects chromatin remodeling with immune activation, including STAT1-associated macrophage responses [44]. MYADM regulates membrane organization and Rac1-dependent cell spreading [45], whereas PREX1 participates in phosphoinositide-dependent Rac signaling and G-protein-coupled receptor trafficking [46]. Gene-centered enrichment in our cohort showed recurring glycosaminoglycan degradation and Fcγ receptor-mediated phagocytosis across the four candidate-associated expression rankings. The tricarboxylic acid cycle was also prominent in the PREX1, MYADM, and KDM6B rankings. Collectively, these observations nominate related membrane-signaling, cellular-metabolic, and selected inflammatory programs for further functional investigation.

Finally, exploratory docking assessed predicted contact interfaces between the four encoded proteins and the antigen-binding variable fragment of erenumab. The experimentally characterized erenumab–CGRP receptor complex provides a structural reference for this work [34]. Candidate-specific interface models, particularly for membrane-associated MYADM, offer defined questions for subsequent localization and binding experiments. Taken

together, the metabolomic, transcriptional, and structural results outline a focused metabolite–transcript framework for studying why patients experience different degrees of improvement during erenumab treatment.

Limitations

Several limitations should be considered. First, this was a single-center discovery cohort of 40 patients, including 14 non-super-responders. Feature screening, UFA-score construction, module selection, and candidate prioritization were all performed in the same patients, increasing the risk of data-dependent findings. The four selected modules met nominal criteria but did not retain significance after correction across all 29 modules. Although the final gene–metabolite associations met Benjamini–Hochberg correction within 84 tests, that correction does not cover the preceding selection steps. Independent validation is therefore necessary before considering these candidates for patient stratification.Second, whole-blood transcriptional signals can reflect variation in leukocyte composition [47], and the analyses did not comprehensively adjust for diet, hormonal factors, concomitant medication, or other possible confounders. The UFA score summarizes relative abundances rather than fatty acid biosynthetic flux. Third, baseline-only sampling and three-month follow-up under one dose regimen preclude assessment of molecular trajectories or longer-term responses. Given the noncausal nature of correlations and the limitations of docking predictions, future studies should prioritize chemical validation, cell-resolved analyses, and independent cohort replication.

Conclusions

In this prospective cohort of Chinese patients with migraine, integrated pretreatment metabolomic and transcriptomic analyses identified an unsaturated fatty acid (UFA)-related metabolic pattern associated with differences in response to erenumab. Cross-omics analysis highlighted four candidate genes showing inverse association with a shared metabolomic feature. Our findings suggest that pretreatment metabolic variation and associated transcriptional patterns may contribute to understanding heterogeneity in erenumab response, providing specific molecular candidates for further investigation.

Abbreviations

BH
Benjamini–Hochberg
CGRP
calcitonin gene-related peptide
CLR
calcitonin receptor-like receptor
DEM
differential metabolite feature
FDR
false discovery rate
FPKM
fragments per kilobase per million mapped reads
Fv
antibody variable fragment
GO
Gene Ontology
GSEA
gene set enrichment analysis
HIT-6
six-item Headache Impact Test
ICHD-3
International Classification of Headache Disorders,third edition
K2EDTA
dipotassium ethylenediaminetetraacetic acid
KEGG
Kyoto Encyclopedia of Genes and Genomes
LC–MS/MS
liquid chromatography–tandem mass spectrometry
MHD
monthly headache days
MIDAS
Migraine Disability Assessment
MSigDB
Molecular Signatures Database
NES
normalized enrichment score
NSR

non-super-responder
PC1
first principal component
QC
quality control
RAMP1
receptor activity-modifying protein 1
RNA-seq
RNA sequencing
SR
super-responder
UFA
unsaturated fatty acid
VIP
variable importance in projection
WGCNA
weighted gene co-expression network analysis.

Declarations

Ethics approval and consent to participate

The study was approved by the Ethics Committee of Tongren Hospital, Shanghai Jiao Tong University School of Medicine (approval number 2025 – 176). Written informed consent was obtained from participants before enrollment. The study was conducted in accordance with the Declaration of Helsinki.

Consent for publication

Not applicable. No identifiable individual participant information is presented.

Competing interests

The authors declare no competing interests.

Funding

This work was supported by the National Natural Science Foundation of China (grant 82571525) and the Shanghai Science and Technology Commission (grant 25DFYCQN).

Author Contribution

Rong Wu and Li Gong conceived the study. Rong Wu contributed to investigation and formal analysis and prepared the first manuscript draft. Jiaqi Fu and Qianfeng Yan contributed to investigation, methodology, and visualization; Qianfeng Yan also contributed to data curation. Tingting Wu contributed to investigation, resources, and validation. Yuanyuan Zeng contributed to investigation, data curation, and software. Xueyuan Liu contributed to manuscript review and editing. Li Gong contributed to supervision, project administration, funding acquisition, and manuscript review and editing.

Acknowledgement

The authors thank the patients who participated in the study and the clinical staff who assisted with enrollment, follow-up, and specimen collection.

Data Availability

Deidentified data and analysis code supporting the reported findings are available from the corresponding authors on reasonable request, subject to institutional approval and participant confidentiality requirements.

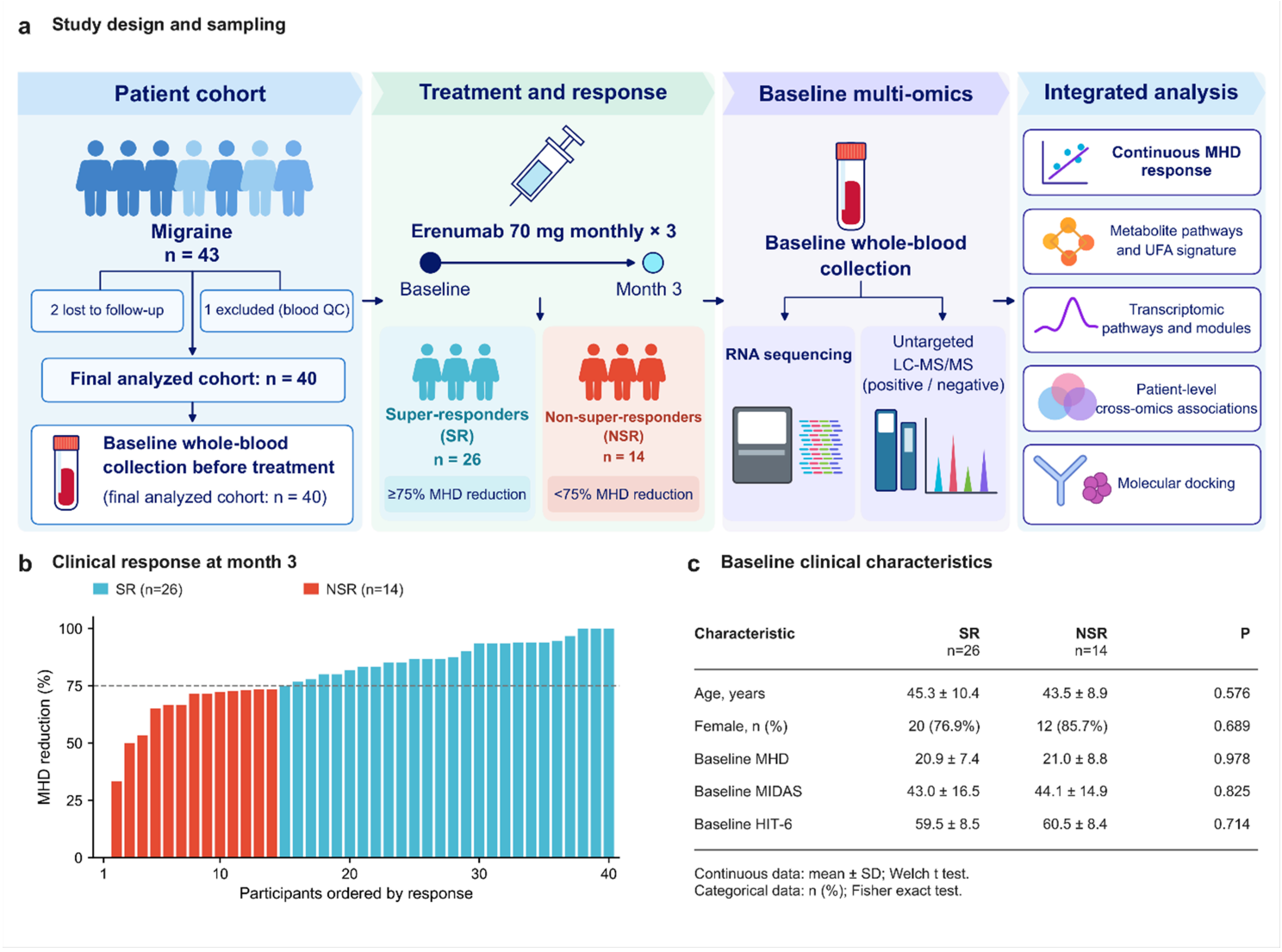
References

1. Ashina M, Migraine (2020) N Engl J Med 383(19):1866–1876. 10.1056/nejmra1915327
2. Novartis China Novartis announces approval of Aimovig in China for the preventive treatment of migraine in adults [Internet; in Chinese]. 2023 Sep 21 [cited 2026 Oct 14]. Available from: https://www.novartis.com.cn/news/nuohuayufangpiantoutongchuangxinyaoanmoweizaizhongguohuopiyongyuchengrenpiantoutongdeyufangxingzhiliao

3. Goadsby PJ, Reuter U, Hallström Y, Broessner G, Bonner JH, Zhang F et al (2017) A Controlled Trial of Erenumab for Episodic Migraine. N Engl J Med 377(22):2123–2132. 10.1056/nejmoa1705848
4. Tepper S, Ashina M, Reuter U, Brandes JL, Doležil D, Silberstein S et al (2017) Safety and efficacy of erenumab for preventive treatment of chronic migraine: a randomised, double-blind, placebo-controlled phase 2 trial. Lancet Neurol 16(6):425–434. 10.1016/s1474-4422(17)30083-2
5. Reuter U, Goadsby PJ, Lanteri-Minet M, Wen S, Hours-Zesiger P, Ferrari MD et al (2018) Efficacy and tolerability of erenumab in patients with episodic migraine in whom two-to-four previous preventive treatments were unsuccessful: a randomised, double-blind, placebo-controlled, phase 3b study. Lancet 392(10161):2280–2287. 10.1016/s0140-6736(18)32534-0
6. Sacco S, Amin FM, Ashina M, Bendtsen L, Deligianni CI, Gil-Gouveia R et al (2022) European Headache Federation guideline on the use of monoclonal antibodies targeting the calcitonin gene related peptide pathway for migraine prevention – 2022 update. J Headache Pain 23:67. 10.1186/s10194-022-01431-x
7. Yu S, Kim BK, Wang H, Zhou J, Wan Q, Yu T et al (2022) A phase 3, randomised, placebo-controlled study of erenumab for the prevention of chronic migraine in patients from Asia: the DRAGON study. J Headache Pain 23:146. 10.1186/s10194-022-01514-9
8. Wang SJ, Roxas AA Jr, Saravia B, Kim BK, Chowdhury D, Riachi N et al (2021) Randomised, controlled trial of erenumab for the prevention of episodic migraine in patients from Asia, the Middle East, and Latin America: The EMPOwER study. Cephalalgia 41(13):1285–1297. 10.1177/03331024211024160
9. Raffaelli B, Fitzek M, Overeem LH, Storch E, Terhart M, Reuter U (2023) Clinical evaluation of super-responders vs. non-responders to CGRP(-receptor) monoclonal antibodies: a real-world experience. J Headache Pain 24:16. 10.1186/s10194-023-01552-x
10. Broessner G, Reuter U, Bonner JH, Dodick DW, Hallström Y, Picard H et al (2020) The Spectrum of Response to Erenumab in Patients With Episodic Migraine and Subgroup Analysis of Patients Achieving ≥ 50%, ≥ 75%, and 100% Response. Headache 60(9):2026–2040. 10.1111/head.13929
11. Brandes JL, Diener HC, Dolezil D, Freeman MC, McAllister PJ, Winner P et al (2020) The spectrum of response to erenumab in patients with chronic migraine and subgroup analysis of patients achieving ≥ 50%, ≥ 75%, and 100% response. Cephalalgia 40(1):28–38. 10.1177/0333102419894559
12. Gross EC, Lisicki M, Fischer D, Sándor PS, Schoenen J (2019) The metabolic face of migraine — from pathophysiology to treatment. Nat Rev Neurol 15(11):627–643. 10.1038/s41582-019-0255-4
13. Ramsden CE, Zamora D, Faurot KR, MacIntosh B, Horowitz M, Keyes GS et al (2021) Dietary alteration of n-3 and n-6 fatty acids for headache reduction in adults with migraine: randomized controlled trial. BMJ 374:n1448. 10.1136/bmj.n1448
14. Langfelder P, Horvath S (2008) WGCNA: an R package for weighted correlation network analysis. BMC Bioinformatics 9(1):559. 10.1186/1471-2105-9-559
15. von Elm E, Altman DG, Egger M, Pocock SJ, Gøtzsche PC, Vandenbroucke JP et al (2007) The Strengthening the Reporting of Observational Studies in Epidemiology (STROBE) Statement: Guidelines for Reporting Observational Studies. PLoS Med 4(10):e296. 10.1371/journal.pmed.0040296
16. Headache Classification Committee of the International Headache Society (IHS). The International Classification of Headache Disorders, 3rd edition. Cephalalgia (2018) ;38(1):1-211. 10.1177/0333102417738202
17. Stewart WF, Lipton RB, Dowson AJ, Sawyer J (2001) Development and testing of the Migraine Disability Assessment (MIDAS) Questionnaire to assess headache-related disability. Neurology 56(6 Suppl 1):S20–S28. 10.1212/wnl.56.suppl_1.s20
18. Kosinski M, Bayliss MS, Bjorner JB, Ware JE Jr, Garber WH, Batenhorst A et al (2003) A six-item short-form survey for measuring headache impact: The HIT-6™. Qual Life Res 12(8):963–974. 10.1023/a:1026119331193
19. Kessner D, Chambers M, Burke R, Agus D, Mallick P (2008) ProteoWizard: open source software for rapid proteomics tools development. Bioinformatics 24(21):2534–2536. 10.1093/bioinformatics/btn323
20. Smith CA, Want EJ, O'Maille G, Abagyan R, Siuzdak G (2006) XCMS: processing mass spectrometry data for metabolite profiling using nonlinear peak alignment, matching, and identification. Anal Chem 78(3):779–787. 10.1021/ac051437y
21. Sumner LW, Amberg A, Barrett D, Beale MH, Beger R, Daykin CA et al (2007) Proposed minimum reporting standards for chemical analysis: Chemical Analysis Working Group (CAWG) Metabolomics Standards Initiative (MSI). Metabolomics 3(3):211–221. 10.1007/s11306-007-0082-2
22. Schrimpe-Rutledge AC, Codreanu SG, Sherrod SD, McLean JA (2016) Untargeted Metabolomics Strategies—Challenges and Emerging Directions. J Am Soc Mass Spectrom 27(12):1897–1905. 10.1007/s13361-016-1469-y
23. Ritchie ME, Phipson B, Wu D, Hu Y, Law CW, Shi W et al (2015) limma powers differential expression analyses for RNA-sequencing and microarray studies. Nucleic Acids Res 43(7):e47. 10.1093/nar/gkv007
24. Thévenot EA, Roux A, Xu Y, Ezan E, Junot C (2015) Analysis of the Human Adult Urinary Metabolome Variations with Age, Body Mass Index, and Gender by Implementing a Comprehensive Workflow for Univariate and OPLS Statistical Analyses. J Proteome Res 14(8):3322–3335. 10.1021/acs.jproteome.5b00354
25. Benjamini Y, Hochberg Y (1995) Controlling the False Discovery Rate: A Practical and Powerful Approach to Multiple Testing. J R Stat Soc Ser B Methodol 57(1):289–300. 10.1111/j.2517-6161.1995.tb02031.x
26. Kanehisa M, Furumichi M, Sato Y, Kawashima M, Ishiguro-Watanabe M (2023) KEGG for taxonomy-based analysis of pathways and genomes. Nucleic Acids Res 51(D1):D587–D592. 10.1093/nar/gkac963
27. Subramanian A, Tamayo P, Mootha VK, Mukherjee S, Ebert BL, Gillette MA et al (2005) Gene set enrichment analysis: a knowledge-based approach for interpreting genome-wide expression profiles. Proc Natl Acad Sci U S A 102(43):15545–15550. 10.1073/pnas.0506580102
28. Wu T, Hu E, Xu S, Chen M, Guo P, Dai Z et al (2021) clusterProfiler 4.0: a universal enrichment tool for interpreting omics data. Innov (Camb) 2(3):100141. 10.1016/j.xinn.2021.100141
29. Chen S, Zhou Y, Chen Y, Gu J (2018) fastp: an ultra-fast all-in-one FASTQ preprocessor. Bioinformatics 34(17):i884–i890. 10.1093/bioinformatics/bty560

30. Love MI, Huber W, Anders S (2014) Moderated estimation of fold change and dispersion for RNA-seq data with DESeq2. Genome Biol 15(12):550. 10.1186/s13059-014-0550-8
31. Liberzon A, Subramanian A, Pinchback R, Thorvaldsdóttir H, Tamayo P, Mesirov JP (2011) Molecular signatures database (MSigDB) 3.0. Bioinformatics 27(12):1739–1740. 10.1093/bioinformatics/btr260
32. Dominguez C, Boelens R, Bonvin AMJJ (2003) HADDOCK: a protein-protein docking approach based on biochemical or biophysical information. J Am Chem Soc 125(7):1731–1737. 10.1021/ja026939x
33. Giulini M, Reys V, Teixeira JMC, Jiménez-García B, Honorato RV, Kravchenko A et al (2025) HADDOCK3: a modular and versatile platform for integrative modeling of biomolecular complexes. J Chem Inf Model 65(13):7315–7324. 10.1021/acs.jcim.5c00969
34. Garces F, Mohr C, Zhang L, Huang CS, Chen Q, King C et al (2020) Molecular insight into recognition of the CGRPR complex by migraine prevention therapy Aimovig (erenumab). Cell Rep 30(6):1714–1723e6. 10.1016/j.celrep.2020.01.029
35. Jumper J, Evans R, Pritzel A, Green T, Figurnov M, Ronneberger O et al (2021) Highly accurate protein structure prediction with AlphaFold. Nature 596(7873):583–589. 10.1038/s41586-021-03819-2
36. Varadi M, Anyango S, Deshpande M, Nair S, Natassia C, Yordanova G et al (2022) AlphaFold Protein Structure Database: massively expanding the structural coverage of protein-sequence space with high-accuracy models. Nucleic Acids Res 50(D1):D439–D444. 10.1093/nar/gkab1061
37. Collins GS, Reitsma JB, Altman DG, Moons KGM (2015) Transparent reporting of a multivariable prediction model for individual prognosis or diagnosis (TRIPOD): the TRIPOD statement. BMJ 350:g7594. 10.1136/bmj.g7594
38. Yu S, Kim BK, Wang H, Zhou J, Banerjee P, Lincy J et al (2026) Long-term safety and continued clinical benefit of erenumab 70 mg in Asian patients with chronic migraine: an open-label extension of the phase 3 DRAGON study. J Headache Pain 27(1):217. 10.1186/s10194-026-02406-y
39. Romozzi M, Lokhandwala A, Vollono C, García-Azorín D, Vigani G, De Cesaris F et al (2025) A nomogram for the prediction of response to anti-CGRP mAbs: the CGRP score. J Headache Pain 26(1):190. 10.1186/s10194-025-02138-5
40. Li S, Tang Y, Fang J, Deng D, Tu Y (2026 Aug) Multi-omics profiling of migraine links plasma proteomic signatures with lipid metabolomic measures. J Headache Pain 24 Online ahead of print. 10.1186/s10194-026-02493-x
41. Hong Y, Chen F, Mi Y, Shu W, Wang Y, Shu Z (2026) Plasma proteomics identifies proteins and pathways associated with incident migraine in 50,668 adults. J Headache Pain 27(1):110. 10.1186/s10194-026-02345-8
42. Lu YZ, Nayer B, Singh SK, Alshoubaki YK, Yuan E, Park AJ et al (2024) CGRP sensory neurons promote tissue healing via neutrophils and macrophages. Nature 628(8008):604–611. 10.1038/s41586-024-07237-y
43. Liu S, Wang H, Li J, Gao J, Yu L, Wei X et al (2024) Loss of Bcl-3 regulates macrophage polarization by promoting macrophage glycolysis. Immunol Cell Biol 102(7):605–617. 10.1111/imcb.12785
44. Huangfu N, Li F, Wang C, Jin S, Zheng X, Wang Y et al (2025) METTL3/RBM15 augments the stability of Kdm6b mRNA and promotes STAT1-mediated macrophage activation and atherosclerosis. Exp Mol Med 57(12):2916–2929. 10.1038/s12276-025-01594-y
45. Aranda JF, Reglero-Real N, Kremer L, Marcos-Ramiro B, Ruiz-Sáenz A, Calvo M et al (2011) MYADM regulates Rac1 targeting to ordered membranes required for cell spreading and migration. Mol Biol Cell 22(8):1252–1262. 10.1091/mbc.e10-11-0910
46. Baker MJ, Hampson E, Islam P, Moral RP, Maunders EA, Hornigold K et al (2025) P-Rex1 limits the agonist-induced internalization of GPCRs independently of its Rac-GEF activity. Cell Rep 44(10):116403. 10.1016/j.celrep.2025.116403
47. O'Connell GC, Wang J, Smothers C (2023) Donor white blood cell differential is the single largest determinant of whole blood gene expression patterns. Genomics 115(6):110708. 10.1016/j.ygeno.2023.110708

Figures



Characteristic	SR n=26	NSR n=14	P
Age, years	45.3 ± 10.4	43.5 ± 8.9	0.576
Female, n (%)	20 (76.9%)	12 (85.7%)	0.689
Baseline MHD	20.9 ± 7.4	21.0 ± 8.8	0.978
Baseline MIDAS	43.0 ± 16.5	44.1 ± 14.9	0.825
Baseline HIT-6	59.5 ± 8.5	60.5 ± 8.4	0.714

Continuous data: mean ± SD; Welch t test.
Categorical data: n (%); Fisher exact test.

Figure 1

Cohort, treatment, and baseline clinical characteristics

(a) Study workflow. Forty-three patients entered the cohort; two were lost to follow-up and one was excluded for sample degradation. The analyzed cohort comprised 40 patients with baseline whole-blood sampling before the first erenumab injection. Erenumab was administered at 70 mg every four weeks, and response was assessed after three months. (b) Individual percentage reduction in monthly headache days (MHD), calculated from the baseline month and month-three count. The 75% threshold defines super-responders (SR; n = 26) and non-super-responders (NSR; n = 14). NSR denotes improvement below this threshold and includes patients with partial clinical benefit. (c) Baseline age, sex, MHD, Migraine Disability Assessment (MIDAS), and Headache Impact Test (HIT-6) summaries. Continuous variables are means ± standard deviations and categorical variables are counts. Baseline probabilities represent descriptive, unadjusted comparisons. All molecular measurements refer to pretreatment specimens.

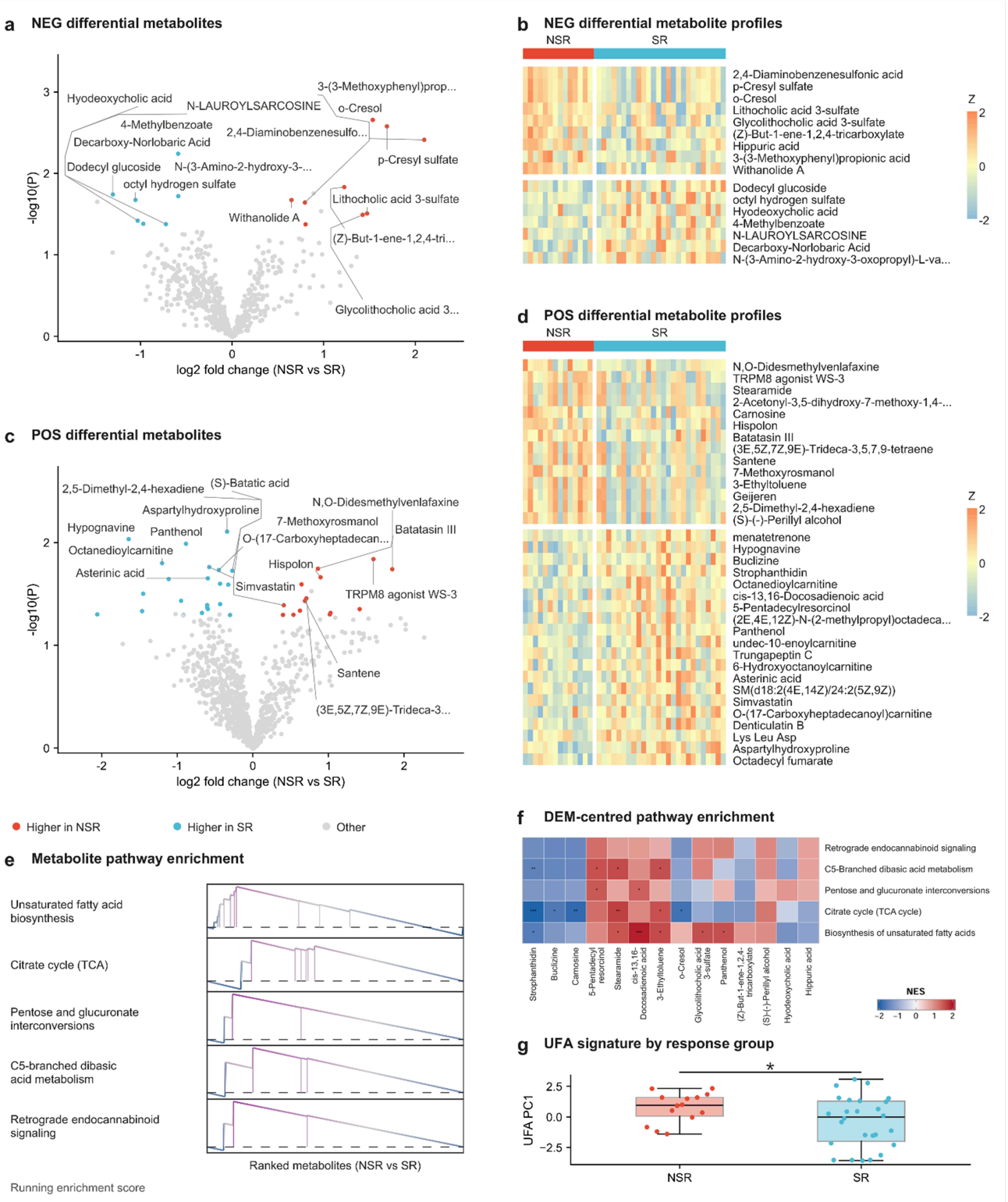
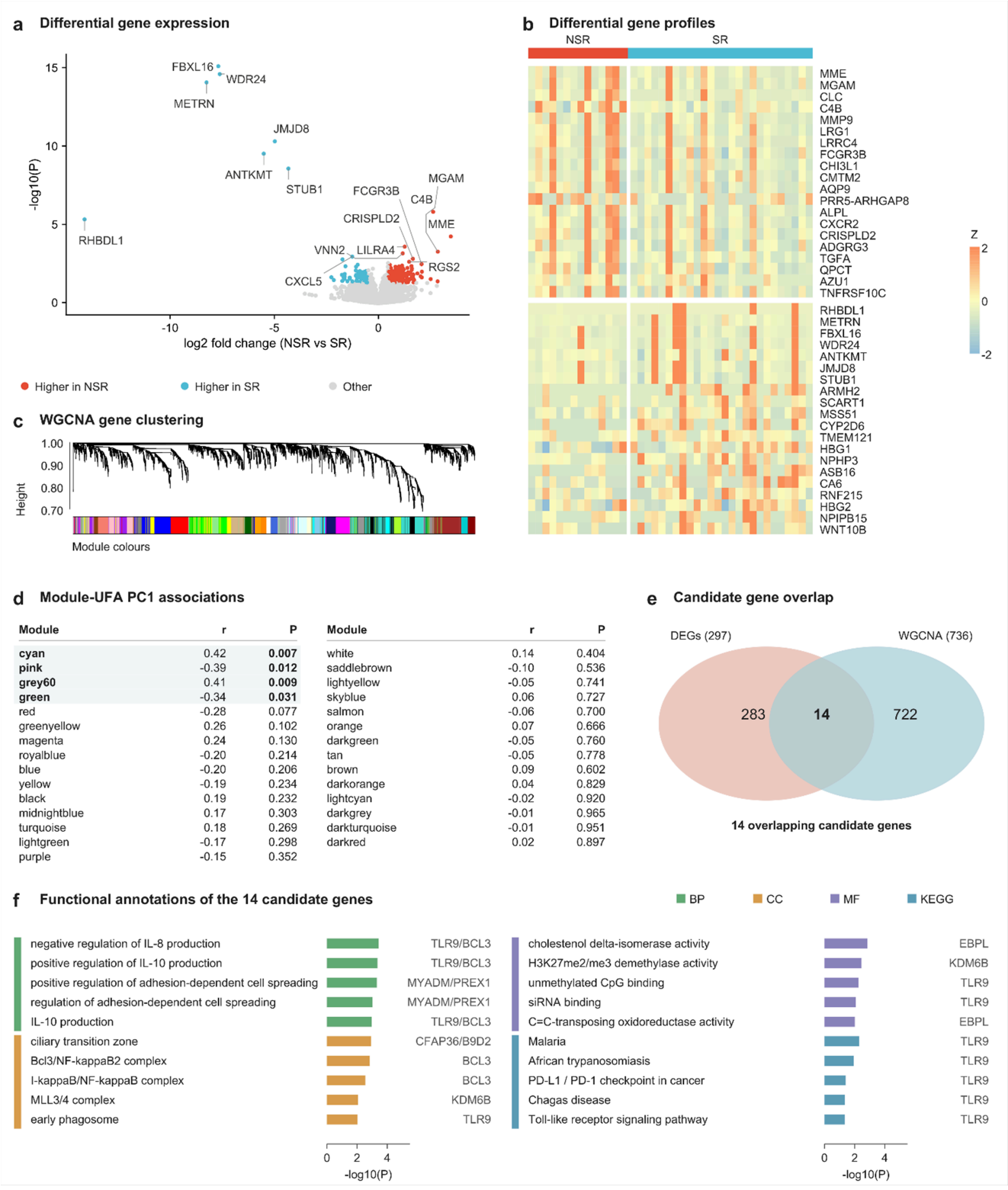


Figure 2

Differential metabolite features and unsaturated fatty acid enrichment

(a, c) Negative- and positive-ion volcano plots for NSR versus SR. Differential metabolite features required VIP >1 and nominal limma P <0.05; positive log2 fold change indicates higher abundance in NSR. Sixteen negative-ion and 36 positive-ion features met this rule. (b, d) Corresponding selected-feature heatmaps, showing row-standardized abundances with colors clipped at ±2. The display limit of 20 features per direction yields 16 negative-ion and 34 positive-ion rows. (e) Phenotype-ranked metabolite set enrichment for the five displayed pathways. (f) Enrichment patterns from differential-metabolite-centered rankings, adjusted for response group. Colors indicate normalized enrichment scores (NES), with red and blue representing positive and negative enrichment, respectively. Asterisks denote nominal enrichment probabilities: *P <0.05, **P <0.01, and ***P <0.001. Pathway coupling does not establish direct pathway membership. (g) UFA score derived from PC1 of the standardized abundances of eight common leading-edge compounds. Each point

represents one participant. Boxes show the median and interquartile range; whiskers extend to the most extreme observations within 1.5 times the interquartile range. The displayed comparison uses a one-sided Wilcoxon rank-sum test (NSR > SR; nominal P = 0.0316; *P < 0.05). The score was derived in the discovery cohort, and the plotted nominal probability is descriptive and data-dependent. UFA biosynthesis had NES = 2.12, P = 0.00118. Pathway displays were selected using nominal criteria. Ion-mode features and provisional compound annotations should not be equated with independently confirmed metabolites. UFA, unsaturated fatty acid; NES, normalized enrichment score; VIP, variable importance in projection.



Module	r	P	Module	r	P
cyan	0.42	**0.007**	white	0.14	0.404
pink	-0.39	**0.012**	saddlebrown	-0.10	0.536
grey60	0.41	**0.009**	lightyellow	-0.05	0.741
green	-0.34	**0.031**	skyblue	0.06	0.727
red	-0.28	0.077	salmon	-0.06	0.700
greenyellow	0.26	0.102	orange	0.07	0.666
magenta	0.24	0.130	darkgreen	-0.05	0.760
royalblue	-0.20	0.214	tan	-0.05	0.778
blue	-0.20	0.206	brown	0.09	0.602
yellow	-0.19	0.234	darkorange	0.04	0.829
black	0.19	0.232	lightcyan	-0.02	0.920
midnightblue	0.17	0.303	darkgrey	-0.01	0.965
turquoise	0.18	0.269	darkturquoise	-0.01	0.951
lightgreen	-0.17	0.298	darkred	0.02	0.897
purple	-0.15	0.352			

Figure 3

Differential expression and UFA-associated transcriptional modules

(a) Transcriptomic volcano plot for NSR versus SR. Exploratory differential expression required nominal DESeq2 P <0.05 and |log2 fold change| >0.5, selecting 297 genes. Positive values indicate higher expression in NSR. (b) Row-standardized expression of up to 20 selected genes in each direction; colors are clipped at ±2. (c) WGCNA gene dendrogram and assigned module colors. (d) Module–UFA score relationships. Cells report biweight midcorrelation and nominal P; module selection used |r| ≥0.30 and P <0.05. Cyan, grey60, pink, and green met these criteria, but none met BH-adjusted P <0.05 across 29 modules. The assigned grey60 module is distinct from the unassigned grey category. (e) Intersection between 297 nominal differentially expressed genes and 736 genes in the four selected modules, yielding 14 candidates. The remaining Venn regions contain 283 and 722 genes, respectively. (f) Displayed GO and KEGG over-representation terms for the 14 genes, selected using nominal probabilities. Gene labels identify the actual annotation support; most displayed KEGG terms depend on TLR9 alone. Disease-named terms indicate shared molecular annotations. WGCNA, weighted gene co-expression network analysis; GO, Gene Ontology; KEGG, Kyoto Encyclopedia of Genes and Genomes.

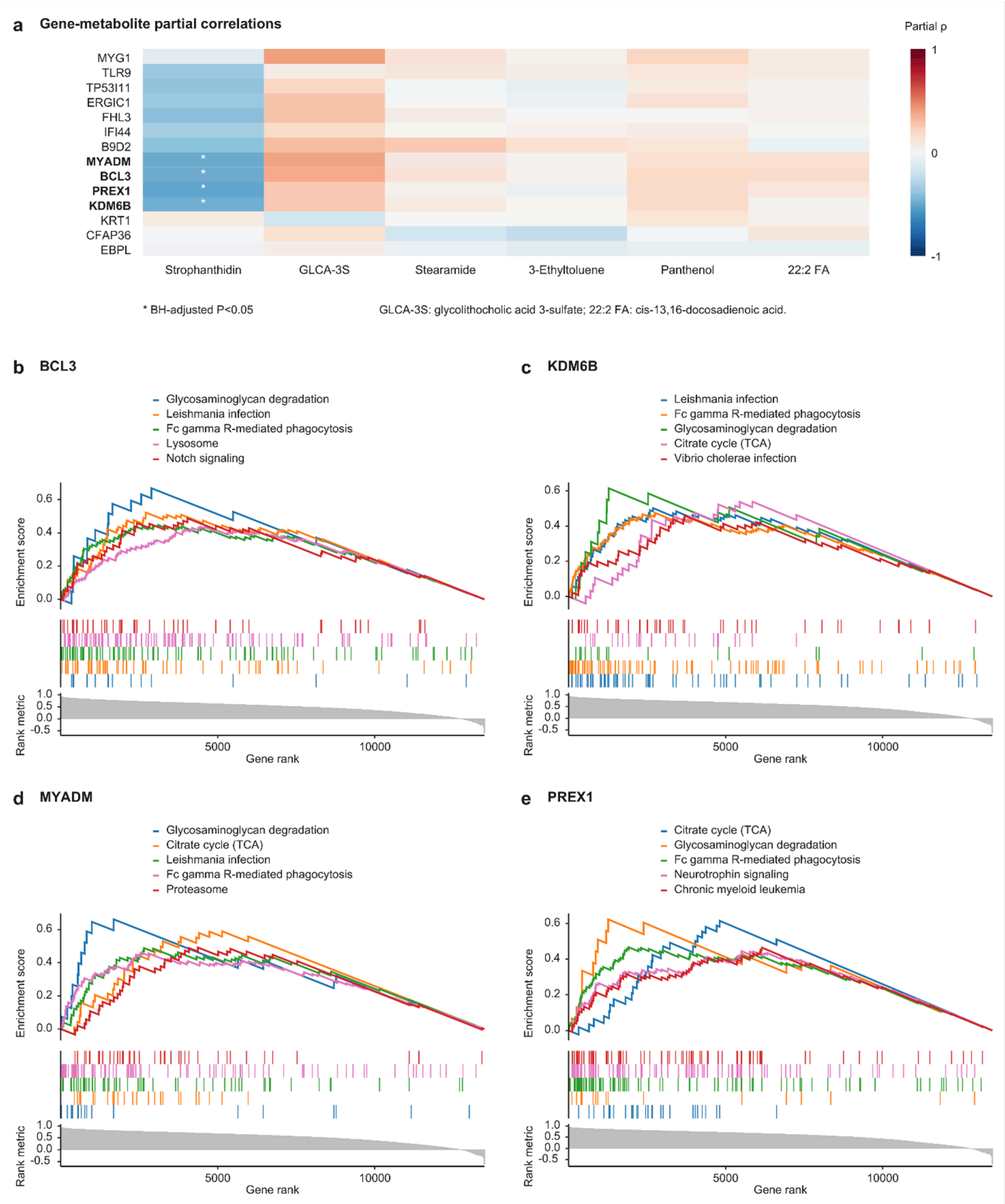


Figure 4

Candidate gene–metabolite associations and gene-centered enrichment

(a) Group-adjusted partial Spearman correlations between 14 candidate genes and six pathway-related differential metabolite features in 40 participants. Correlations were calculated between rank residuals after regression on response group. The six-feature set includes one direct UFA pathway member and five features linked by DEM-centered enrichment. BH adjustment covered all 84 pairs. Asterisks identify P <0.05; candidate prioritization additionally required |partial rho| >0.40. The feature Com_1326_pos, provisionally annotated as strophanthidin, was inversely associated with PREX1, MYADM, BCL3, and KDM6B (partial rho −0.517, −0.497, −0.485, and −0.480; P = 0.0418 each). (b–e) Gene-centered KEGG legacy set enrichment for BCL3, KDM6B, MYADM, and PREX1, respectively. Genes were ranked by their expression correlation with the indicated candidate across the cohort; these rankings were not adjusted for response group. The five largest absolute NES values among pathways with P <0.05 are displayed for each candidate. Gene-centered enrichment describes co-expression context, not demonstrated regulation by the candidate. The strophanthidin annotation remains subject to chemical confirmation and does not denote direct membership in UFA biosynthesis.

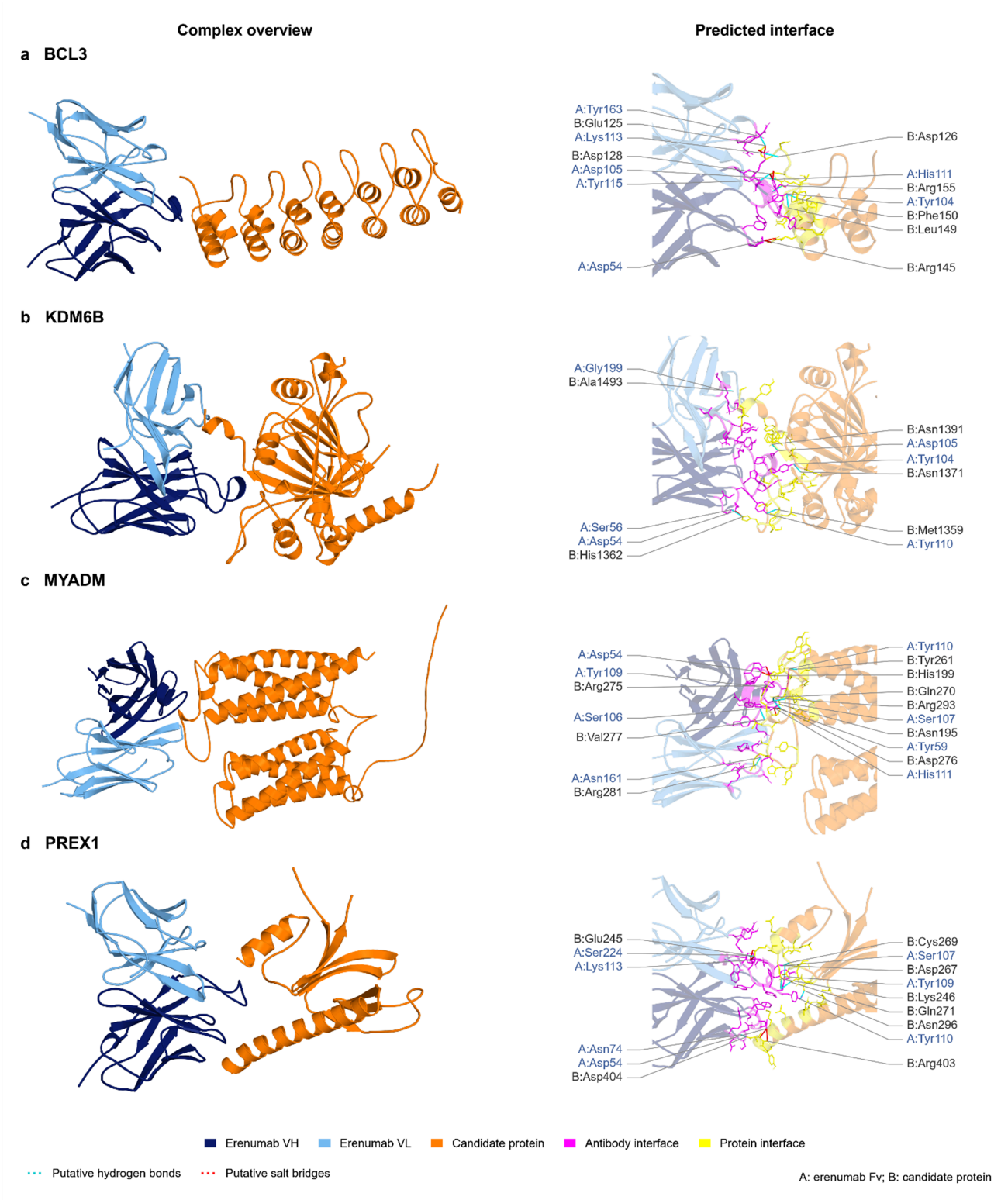


Figure 5

Exploratory structural assessment of four candidate proteins with erenumab

Structural visualizations of four candidate proteins with the erenumab variable fragment: (a) BCL3, (b) KDM6B, (c) MYADM, and (d) PREX1. Overview and enlarged interface views are shown. BCL3, KDM6B, and PREX1 inputs represent available structural domains; MYADM uses an AlphaFold-derived full-length model. The antibody Fv comprises variable domains from PDB 6UMG and lacks the complete IgG2 architecture. Residue numbers follow the input coordinates and may differ from canonical numbering. Dashed contacts and hydrogen-bond or salt-bridge labels represent geometric predictions for experimental assessment.